MALAYSIAN JOURNAL OF MICROSCOPY

Journal homepage: https://malaysianjournalofmicroscopy.org

RESEARCH ARTICLE

SYNTHESIS OF SAGO-BARK BASED ACTIVATED CARBON VIA MICROWAVE ACTIVATION FOR AMOXICILLIN REMOVAL: OPTIMIZATION VIA RESPONSE SURFACE METHODOLOGY

Siti Zawiyah Baharom, Erniza Mohd Johan Jaya, Mohd Azmier Ahmad*

School of Chemical Engineering, Engineering Campus, Universiti Sains Malaysia, 14300 Nibong Tebal, Pulau Pinang, Malaysia.

Abstract. Antibiotics such as amoxicillin (AMOX), when introduced into water bodies due to inadequate wastewater treatment, can pose serious environmental risks, affecting aquatic life. This concern led to the present study aimed at synthesizing sago bark-based activated carbon (SBAC) for the adsorption of AMOX from water. SBAC was prepared using a combined physicochemical activation process, which involved chemical activation with potassium hydroxide (KOH) and subsequent microwave-assisted physical activation using carbon dioxide (CO_2) gas. The optimization of SBAC synthesis was realized harnessing response surface methodology (RSM) with a central composite design (CCD). The optimal conditions identified were 556.41 watts for radiation power, 6.06 minutes for activation time, and a KOH impregnation ratio (IR) of 1.76 g/g. Under these conditions, AMOX uptake and SBAC yield were optimized at 75.65 mg/g and 31.54%, respectively. The models accurately predicted actual values of 77.59 mg/g for AMOX uptake and 32.56% for SBAC yield, with low errors of 2.50% and 3.13%, confirming the models' reliability. The uptake of AMOX was primarily swayed by radiation power, followed by IR, while the yield of SBAC was mostly governed by radiation power, succeeded by activation time. Scanning electron microscopy (SEM) analysis revealed that the raw sago bark had a non-porous structure, whereas the activation process created a highly porous SBAC surface, demonstrating the effectiveness of the activation methods. Isotherm analysis indicated that AMOX adsorption onto SBAC followed the Freundlich model, achieved an adsorption capacity (Q_m) of 110.52 mg/g, suggesting multilayer adsorption on a heterogeneous surface. Overall, the findings highlight that SBAC is an efficient, low-cost, and sustainable adsorbent for mitigating antibiotic pollution in aquatic environments.

Keywords: Antibiotic adsorption, activated carbon, microwave-assisted activation, response surface methodology, central composite design

Article Info

Received 20 April 2025
Accepted 22 October 2025
Published 4 December 2025

***Corresponding author: chazmier@usm.my**

ISSN: 1823-7010, eISSN: 2600-7444

1. INTRODUCTION

Amoxicillin (AMOX), a commonly prescribed broad-spectrum antibiotic, is extensively utilized in the treatment of bacterial infections due to its efficacy and affordability [1]. The extensive use of AMOX has resulted in its frequent detection in wastewater, surface water, and groundwater. Large portions are excreted unchanged, leading to environmental contamination via improper disposal and agricultural runoff. Conventional treatment systems often fail to remove AMOX completely, allowing its persistence in aquatic environments. For instance, nanofiltration is another common method to treat antibiotic wastewater, offering strong adsorption affinity but easily affected by solution chemistry, organic matter, and salinity [2]. Ozonation and titanium dioxide (TiO_2) photocatalysis are advanced oxidation processes widely applied for antibiotic degradation. Despite their efficiency, these processes are constrained by high operational costs, complex reaction mechanisms, and the limitations associated with extensive ozone usage [2]. This persistence can disrupt aquatic ecosystems by affecting the growth and reproduction of non-target organisms. Additionally, the continuous exposure of environmental microbes to residual AMOX can accelerate the evolution of antibiotic-resistant bacteria, a critical concern for public health [3]. Adsorption is a surface process where adsorbates adhere to a solid adsorbent through physical or chemical interactions, effectively removing pollutants like antibiotics [4], dyes [5], heavy metal [6] and so on, from water. It offers simplicity, high efficiency, and cost-effectiveness [7]. Activated carbon (AC), commonly used for adsorption, is typically derived from coal, a non-renewable source with environmental and cost issues. Due to this, scientists are keen to produce AC from agricultural wastes including jackfruit peel [8], coconut shell [9] and others. AC serves as a superior adsorbent compared to other materials because its adsorption performance is primarily influenced by its large surface area, which provides numerous active sites for the attachment of adsorbate molecules [10].

Recently, enhancing AC production has become a critical research priority, given the multiple factors influencing optimal performance. Response Surface Methodology (RSM) provides a statistical approach for efficient multivariable optimization and process modelling [11]. Central Composite Design (CCD) is a preferred RSM approach as it minimizes experimental runs, captures variable interactions, and develops predictive models. Three-dimensional (3D) plots visualize parameter effects, while result accuracy and significance are verified through analysis of variance (ANOVA). [10]. Microwave irradiation grants multiple benefits in contrast to conventional pyrolysis, involving faster and uniform heating, shorten processing duration, and boosted energy effectiveness due to direct internal energy transfer [12]. Microwave heating allows precise temperature control, yielding higher product quality and reduced energy loss. It also lowers greenhouse emissions and enables selective heating that enhances activation and pore development in AC [13].

In this study, AC was produced from sago bark using a microwave activation technique and further optimized with RSM for the clearance of AMOX from aqueous solutions. The sago tree (*Metroxylon sago*) is well-known for its production of sago flour and is considered an economically significant crop in several countries, such as Malaysia, Indonesia, the Philippines, and New Guinea [14]. Sago bark, a plentiful agricultural byproduct with an estimated yearly yield of 20 kilotons in Malaysia, offers a sustainable and environmentally friendly alternative [15]. This work directly supports the United Nations Sustainable Development Goals (SDGs), particularly SDG 6 (Clean Water and Sanitation) and SDG 12 (Responsible Consumption and Production), by promoting clean water restoration and the sustainable valorisation of agricultural waste. Despite extensive research on AC derived from various biomass sources, studies focusing on sago bark-based AC for AMOX removal remain scarce. The integration of microwave-assisted activation with statistical optimization through RSM provides a novel and systematic approach to enhance adsorption efficiency and yield. Therefore, the primary aim of this study is to develop and optimize SBAC for the effective removal of AMOX from water, optimize its yield, and evaluate its characteristics and adsorption isotherm behaviour.

2. MATERIALS AND METHODS

2.1 Materials and SBAC Preparation

Sago bark, sourced from Mukah, Sarawak, Malaysia, was used as the raw precursor. Potassium hydroxide, KOH pellets (85% purity) and hydrochloric acid, HCl were provided by Sigma-Aldrich. High-purity nitrogen (N_2) and carbon dioxide (CO_2) gases (99.99% purity) were delivered by MOX Gases Berhad, Malaysia. The sago bark precursor was thoroughly rinsed via tap water and then air-dried in a controlled environment for approximately 48 hours. It was then subjected to pyrolysis at 550 °C for 1.5 hours in a steady stream of N_2 gas, resulting in char formation. After carbonization, the char was cooled using an inert N_2 gas flow to prevent oxidation and preserve its specific properties. The cooled pyrolyzed sample (char) was later treated with KOH at an impregnation ratio (IR) ranging from 0.5 to 2.0 g/g for 24 hours. The impregnated samples were dried and subsequently activated in a microwave oven at radiation power levels from 264 to 616 watts for durations between 2 and 20 minutes. During the activation process, CO_2 gas was introduced at a steady flow rate of 150 cm^3/min [7]. These parameters were selected based on preliminary experiments and literature evidence indicating that this range effectively promotes pore formation while preventing structural collapse or excessive burn-off. The combined KOH–CO_2 activation allows chemical and physical activation synergy, enhancing surface area and functional group development suitable for antibiotic adsorption.

2.2 Optimization Investigation

For optimization purposes, the dataset was processed by exploiting Design Expert Program (v. 12, STAT-EASE Inc., Minneapolis, USA). The study employed a Central Composite Design (CCD) under the Response Surface Methodology (RSM) to scrutinize the repercussion of three independent factors: radiation power (X_1), radiation time (X_2), and IR (X_3). The evaluation focused on two key responses: the AMOX uptakes (Y_1) and the yield of SBAC (Y_2). The experimental ranges for the variables were defined with levels of +1, 0, and -1, corresponding to radiation power settings of 264, 440, and 616 watts; durations of 4, 12, and 20 minutes; and IR of 0.50, 1.25, and 2.0 g/g, respectively. The optimization ranges for these parameters were carefully selected based on preliminary screening experiments and literature reports to ensure that the chosen levels adequately captured both the lower and upper bounds of the process performance [7]. The RSM optimum conditions were verified by setting the variables “within the studied range” and defining the responses as “maximum” in the Design Expert software to confirm the model’s prediction accuracy. Since the microwave instrument allowed only discrete power settings (264, 440, 616, and 700 watts), the optimal effective power of 556.41 watts was achieved by interpolation through time adjustment. The sample was irradiated for 4.00 min at 616 watts and 2.06 min at 440 watts (total = 6.06 min), yielding an average power equivalent to 556.41 watts.

2.3 Characterization Methods

The investigation thoroughly assessed the physicochemical properties of the samples, including surface area (via BET analysis), mesoporous characteristics, pore size distribution, and total pore volume. These evaluations were conducted using a Micromeritics ASAP 2010 volumetric adsorption analyzer. Prior to analysis, the samples were degassed at 200 °C for 4 h under vacuum, and nitrogen adsorption–desorption isotherms were obtained at 77 K. The BET method was applied to determine the specific surface area, while the BJH (Barrett–Joyner–Halenda) model was used to evaluate the pore size distribution and total pore volume. Elemental composition was determined using a Perkin Elmer Series II 2400 analyzer (USA). Combustion was carried out at 950 °C under oxygen flow to quantify C, H, N, and O contents. Furthermore, surface morphology was examined through scanning electron microscopy (SEM) imaging, utilizing a Quanta 450 FEG microscope (Netherlands) to capture detailed structural features. The SEM was operated at an accelerating voltage of 15 kV, and all powdered samples were gold-sputtered for 60 s to enhance image contrast and surface conductivity. These techniques elucidate

pore structure, surface chemistry, and morphology, providing comprehensive insight into activation effects and adsorption performance of SBAC.

2.4 Isotherm Investigation

For the isotherm study, Erlenmeyer flasks were prepared with six distinct initial concentrations of AMOX (C_o), specifically at 10, 20, 40, 60, 80, and 100 mg/L. These containers were placed in a water bath shaker. The experimental conditions, including the solution volume (200 mL), the mass of optimized SBAC (0.20 g), and the temperature (30 °C), were maintained consistently throughout. After reaching equilibrium, the saturation of AMOX (C_e) was deduced using a UV-Vis spectrophotometer (Agilent Cary 60, USA). The contact time for the adsorption test was set at 6 h, during which the concentration of AMOX no longer changed, indicating that equilibrium had been achieved. The concentration of AMOX was determined using a UV–Vis spectrophotometer at a wavelength of 295 nm [16]. Below was the formula to deduce the quantity of adsorbed AMOX at the phase of equilibrium, (q_e, mg/g):

$$q_e = \frac{(C_o - C_e)V}{W} \tag{1}$$

The experimental data were inspected with several models, and the corresponding equations for each model are presented [17]:

Langmuir:

$$q_e = \frac{Q_m K_L C_e}{1 + K_L C_e} \tag{2}$$

Freundlich:

$$q_e = K_F C_e^{1/n_F} \tag{3}$$

Temkin:

$$q_e = \frac{RT}{B} \ln(AC_e) \tag{4}$$

the constants in these models were explained clearly in [4]. The root mean square error (RMSE) and error percentage are computed using Equation (5) and (6), respectively:

$$RMSE = \sqrt{\frac{1}{n-1}} \sum_{n=1}^{n} \left(q_{e,exp,n} - q_{e,cal,n}\right)^2 \tag{5}$$

$$Error\ (\%) = \frac{(q_{e,exp} - q_{e,cal})}{q_{e,exp}} \times 100\% \tag{6}$$

3. RESULTS AND DISCUSSION

3.1 Optimization Process

3.1.1 Regression Models Development

Table 1 presents the experimental design framework for synthesizing the optimized SBAC. The AMOX uptake ranged from 35.39 to 88.39 mg/g, while the SBAC yield varied between 13.22% and 38.96%. The quadratic models in coded variables effectively predicted both responses based on the input parameters, as shown in Equations (7) and (8) for AMOX uptake (Y_1) and SBAC yield (Y_2), respectively. Quadratic models are frequently employed in RSM because they can accurately represent variable relationships in systems that demonstrate curvature. In contrast to linear models, which assume a direct proportionality between factors and responses, quadratic models include both squared and interaction terms. These additional components enable the exploration of nonlinear and more intricate relationships. Consequently, quadratic models are particularly advantageous in optimization studies, as they allow for the evaluation of not only the primary effects of individual variables but also their combined and higher-order influences [7].

AMOX uptakes (mg/g), Y_1

$$Y_1 = 64.85 + 16.14X_1 + 4.74X_2 + 5.24X_3 + 1.29X_1X_2 + 3.31X_1X_3 - 0.7850X_2X_3 - 7.10X_1^2 - 6.10X_2^2 + 6.00X_3^2 \quad (7)$$

SBAC yield (%), Y_2

$$Y_2 = 33.80 - 5.92X_1 - 5.12X_2 + 1.63X_3 - 2.00X_1X_2 - 0.5750X_1X_3 - 1.07X_2X_3 + 1.08X_1^2 - 1.66X_2^2 - 6.69X_3^2 \quad (8)$$

Table 1: Thorough experimental design layout for optimized SBAC preparation

Run	SBAC preparation variables			Responses	
	Radiation power, X_1 (°C)	Radiation time, X_2 (minutes)	IR, X_3 (g/g)	AMOX uptakes, Y_1 (mg/g)	SBAC yield, Y_2 (%)
1	616	20	0.50	74.02	13.96
2	440	11	1.25	62.86	33.25
3	264	2	2.00	39.66	38.96
4	264	2	0.50	35.39	33.12
5	264	20	2.00	44.44	30.99
6	440	11	1.25	64.51	33.98
7	616	2	2.00	76.52	29.65
8	440	11	1.25	65.33	34.27
9	440	11	1.25	66.35	34.85
10	440	20	1.25	60.99	25.54
11	264	11	1.25	42.98	38.59
12	616	2	0.50	60.92	25.64
13	440	11	0.50	59.73	23.44
14	264	20	0.50	45.22	28.96
15	616	11	1.25	69.22	28.96
16	440	11	2.00	78.66	28.55
17	440	11	1.25	67.44	35.19
18	440	11	1.25	69.23	35.74
19	440	2	1.25	53.21	36.52
20	616	20	2.00	88.39	13.22

Figures 1(a) and (b) illustrate the regression plots comparing the predicted and actual values for AMOX uptake and SBAC yield, respectively. The R^2 and adjusted R^2 (adj-R^2) values were 0.9675 and 0.9383 for AMOX uptake, and 0.9781 and 0.9583 for SBAC yield. These high R^2 and adj-R^2 values demonstrate a strong fit of the regression models, effectively capturing the majority of the variability in the dependent responses. Additionally, the standard deviations (SD) were low, measured at 3.48 for AMOX uptake and 1.45 for SBAC yield, indicating a precise model fit and minimal error in the predictions. The adequate precision (AP) values for AMOX uptake and SBAC yield were determined to be 21.21 and 26.65, respectively. As both values exceed the threshold of 4, the models exhibit a strong signal-to-noise ratio, confirming their reliability in accurately predicting the responses [18].

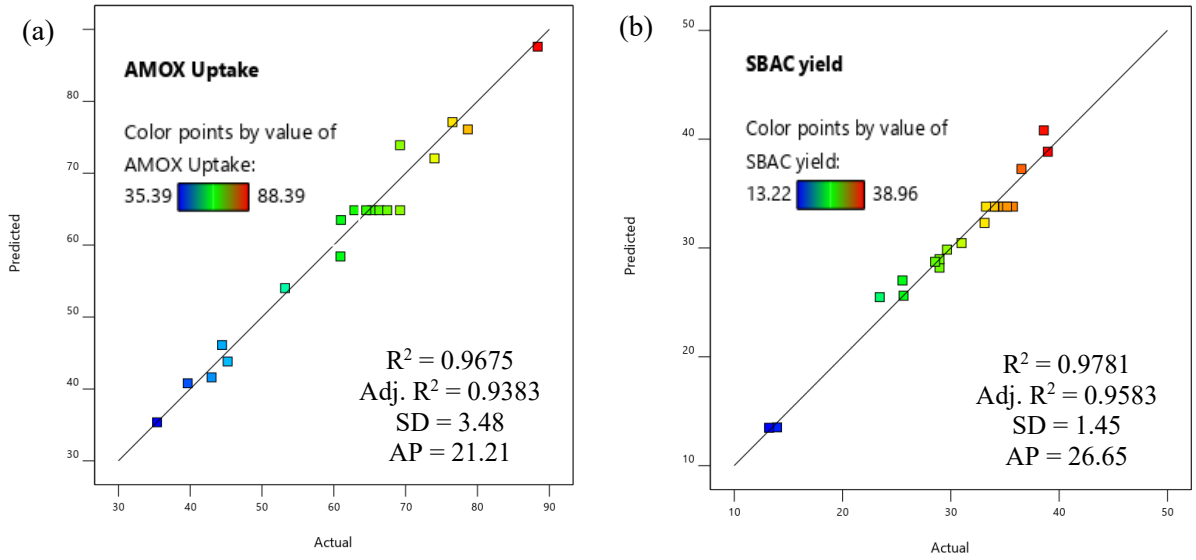

Figure 1: Regression plots for (a) AMOX update and (b) SBAC yield

3.1.2 Analysis of Variance (ANOVA)

Table 2 summarizes the analysis of variance (ANOVA) results for the responses. Both responses exhibited p-values less than 0.0001, confirming their statistical significance.

Table 2: ANOVA results for AMOX uptakes and SBAC yield responses

Source	Response 1, Y_1: AMOX uptakes by SBAC					Response 2, Y_2: SBAC yield				
	Sum of Squares	DF	Mean Square	F Value	p-value	Sum of Squares	DF	Mean Square	F Value	p-value
Model	3611.39	9	401.27	33.09	< 0.0001	938.90	9	104.32	49.58	< 0.0001
X_1	2604.35	1	2604.35	214.78	< 0.0001	350.35	1	350.35	166.49	< 0.0001
X_2	224.30	1	224.30	18.50	0.0016	262.35	1	262.35	124.67	< 0.0001
X_3	274.47	1	274.47	22.64	0.0008	26.41	1	26.41	12.55	0.0053
X_1X_2	13.42	1	13.42	1.11	0.3176	31.92	1	31.92	15.17	0.0030
X_1X_3	87.65	1	87.65	7.23	0.0228	2.64	1	2.64	1.26	0.2884
X_2X_3	4.93	1	4.93	0.4066	0.5381	9.16	1	9.16	4.35	0.0635
X_1^2	138.49	1	138.49	11.42	0.0070	3.24	1	3.24	1.54	0.2432
X_2^2	102.21	1	102.21	8.43	0.0157	7.58	1	7.58	3.60	0.0870
X_3^2	98.96	1	98.96	8.16	0.0171	123.26	1	123.26	58.58	< 0.0001

For AMOX uptake, significant model terms were identified as X_1, X_2, X_3, X_1X_3, X_1^2, X_2^2, and X_3^2. Regarding SBAC yield, the significant factors included X_1, X_2, X_3, X_1X_2, and X_3^2. The F-values indicate that AMOX uptake was predominantly influenced by radiation power (98.27) and impregnation ratio (22.64), while SBAC yield was mainly affected by radiation power (166.49) and radiation time (124.67).

3.1.3 Three-dimensional (3D) Contour Plot

Figure 2(a) shows a 3D plot illustrating the combined effects of radiation power and IR on AMOX uptake, while Figure 2(b) depicts the influence of radiation power and radiation time on SBAC yield.

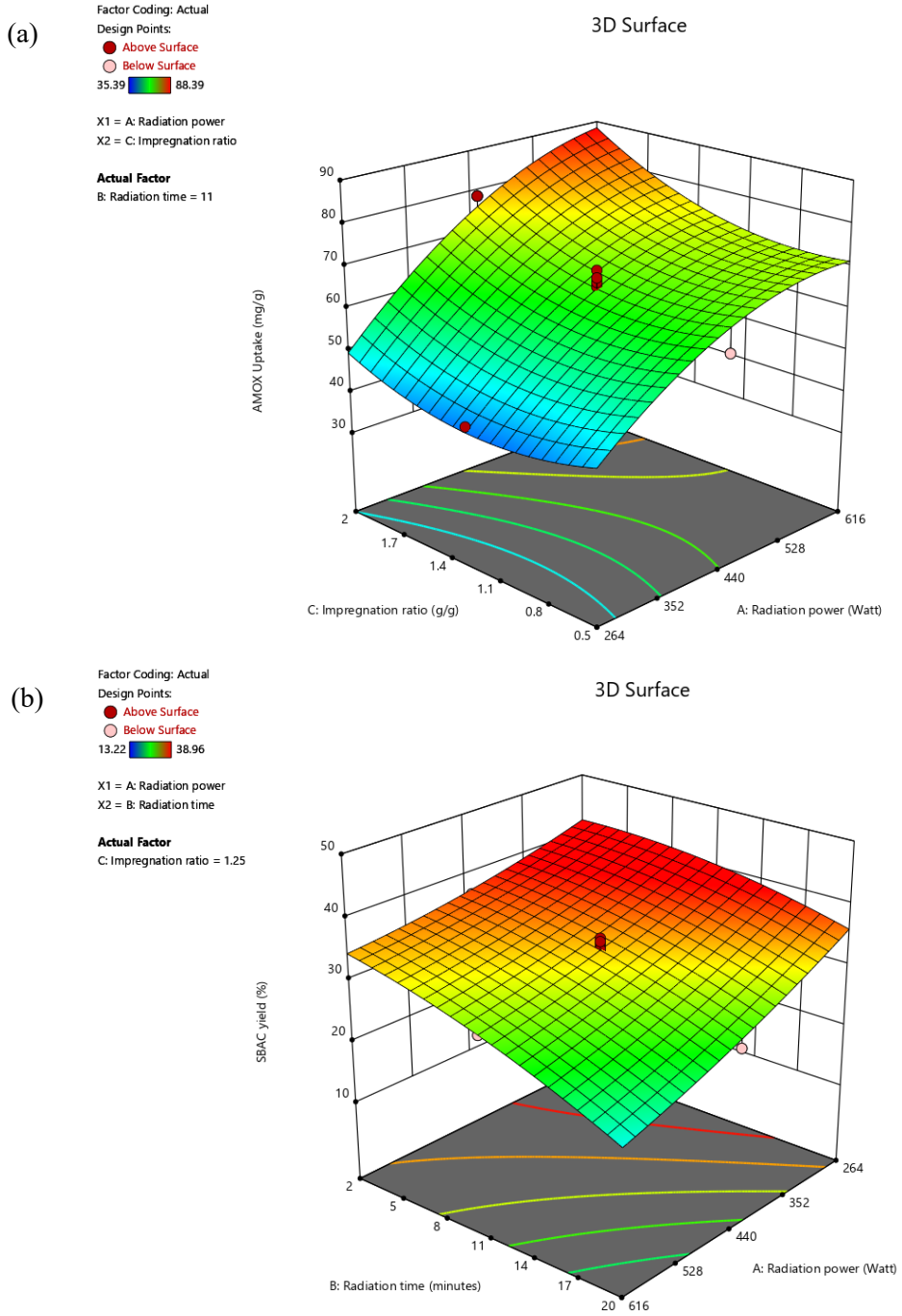

Figure 2: 3D surface plots for (a) AMOX uptakes and (b) SBAC yield

The highest AMOX uptake (88.39 mg/g) occurred at 616 watts and an IR of 2.00 g/g, indicating a strong positive interaction. Increasing radiation power from 264 to 616 watts significantly enhanced AMOX uptake within the IR range of 1.11 – 2.00 g/g, confirming the synergistic effect of these factors. Higher radiation power improved heating efficiency, facilitating volatile removal, pore formation, and surface area development, which enhanced adsorption capacity [19]. Similarly, a higher IR resulted in an increased concentration of K^+ ions, which enhanced their penetration into the material's matrix, thereby promoting more extensive pore formation [20]. Figure 2(b) shows that the minimum SBAC yield of 13.22% was observed at the uppermost radiation power of 616 watts and the longest radiation time of 20 minutes, indicating a detrimental effect of these parameters on yield. As radiation time increased from 12 to 20 minutes, the reduction in SBAC yield became more evident, particularly at radiation power levels between 440 and 616 watts. The combined increase in both radiation power and time intensified thermal cracking, leading to a greater loss of material components and consequently resulting in a lower yield [10].

The optimal conditions for the variables and responses were determined by minimizing the input variables while maximizing the target responses. RSM revealed that the optimum variables were 556.41 watts, 6.06 minutes, and 1.76 g/g for radiation power, radiation time, and IR, respectively. These conditions corresponded to optimum responses of 75.65 mg/g for AMOX uptake and 31.54% for SBAC yield. The actual response values were 77.59 mg/g and 32.56%, resulting in low error percentages of 2.50% and 3.13%, respectively. The small difference observed between the predicted and experimental values underscores the precision and dependability of the established models in forecasting response behaviour under optimal conditions. This outcome verifies the strength of the optimization strategy, illustrating its capability to deliver highly accurate predictions for effective process optimization [12].

3.2 Characteristics of Samples

3.2.1 Surface Area and Pores Characteristic

Table 3 summarizes the surface area and pore characteristics of the samples. The precursor showed a very low BET surface area (2.11 m^2/g) and total pore volume (0.0001 cm^3/g), with no detectable mesoporosity. After carbonization and activation, the optimized SBAC exhibited major improvements, achieving a BET surface area of 1011.93 m^2/g, mesopore surface area of 738.65 m^2/g, and total pore volume of 0.3481 cm^3/g. The average pore diameter increased from 2.24 to 2.79 nm due to KOH activation and CO_2 gasification. KOH expanded the pore network, while CO_2 bombardment further enhanced surface development, consistent with previous findings for teak oil palm trunk-based activated carbon [7]. During activation, heated CO_2 molecules collided with and etched the carbon surface, creating micro- and mesopores that increased the surface area, pore volume, and average pore width [8]. In parallel, the interaction of CO_2 with KOH generated potassium carbonate (K_2CO_3), which acted as a reactive and mobile species. Upon heating, this compound acquired sufficient kinetic energy to diffuse deeply into the carbon matrix, facilitating internal pore expansion and additional structural modification. As a result, the SBAC exhibited a more developed porous framework with significantly improved textural properties [8].

Table 3: Surface area and pore characteristics

Samples	BET surface area (m^2/g)	Mesopores surface area (m^2/g)	Total pore volume (cm^3/g)	Average pore diameter (nm)
Precursor	2.11	-	0.0001	-
Char	489.63	318.86	0.2146	2.24
SBAC	1011.93	738.65	0.3481	2.79

3.2.2 Elemental and Proximate Analysis

The precursor exhibited a substantial elemental carbon (C) content of 30.59%, which is relatively high and comparable to other biomasses successfully converted into AC, such as rattan waste (34.52%) [10] and orange peel (33.44%) [16]. After carbonization and activation, the carbon content in SBAC increased significantly to 70.89%, indicating the successful conversion of organic matter into a carbon-rich structure. In contrast, the proportions of hydrogen (H), nitrogen (N), sulfur (S), and oxygen (O) decreased from 4.15% to 3.21%, 0.44% to 0.22%, 0.29% to 0.17%, and 64.53% to 25.51%, respectively. Proximate analysis confirmed a notable reduction in moisture content and volatile matter, decreasing from 6.69% to 2.51% and from 65.64% to 23.07%, respectively. This decline demonstrates the effective elimination of water and thermally unstable components such as cellulose, hemicellulose, lignin, and tar through evaporation and thermal decomposition [7]. The fixed carbon content increased remarkably from 24.56% to 72.19%, reflecting the formation of a stable carbon framework that supports pore structure and enhances mechanical stability [7]. The ash content decreased from 3.11% to 2.23%, indicating fewer non-porous residues that hinder adsorption. Together with higher fixed carbon and lower volatiles, this confirms effective enhancement of SBAC's purity, structure, and adsorption capacity [8]. The rise in carbon and fixed carbon content aligns with the improved surface area and pore formation in Section 3.2.1. High fixed carbon ensured structural stability, while reduced volatiles created more channels, confirming the elemental enhancement behind SBAC's superior texture and structure.

3.2.3 SEM Images

Figure 3 presents the SEM images of the samples. In Figure 3(a), the precursor's surface appears compact and lacks visible pores, consistent with the expected presence of lignin, cellulose, hemicellulose, and tar. In contrast, Figure 3(b) reveals that the optimized SBAC exhibits a highly porous surface with numerous empty cavities. Initially occupied by moisture and volatile compounds, these components evaporated and escaped during carbonization. The subsequent chemical activation, driven by KOH infiltration and CO_2 gasification, further facilitated the development of pores.

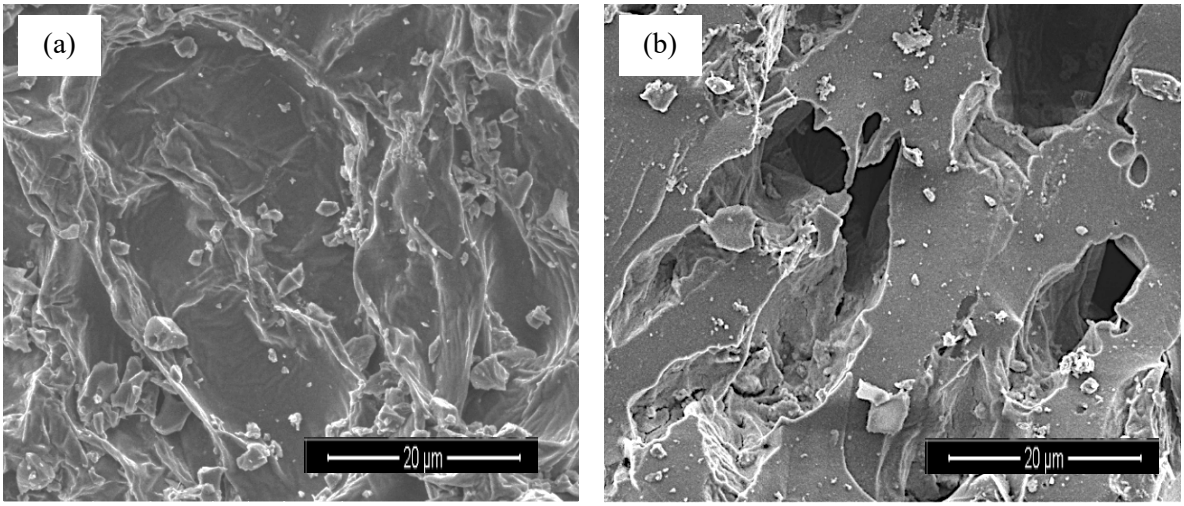

Figure 3: SEM images of (a) sago bark and (b) SBAC at magnification level of 5000×

3.3 Adsorption Isotherm

Figure 4 shows the isotherm plots for AMOX-SBAC adsorption system at 30 °C whilst Table 4 provides a detailed summary of the derived isotherm model parameters. Based on the evaluation of RMSE and error percentage, the Freundlich model was the most accurate in describing the AMOX

adsorption onto SBAC, showing the lowest RMSE of 1.58 and an error of 6.56%. The Freundlich model implies that AMOX adsorption on the OPTAC surface involves multilayer formation. The heterogeneity factor, n_F, was between 1 and 10, signifying a favourable adsorption process [21]. The maximum adsorption capacity, Q_m, was notably high of 110.52 mg/g. In comparison, SBAC demonstrated superior AMOX removal performance relative to other adsorbents, including hybrid AC/maltodextrin-functionalized fibrous silica (77.31 mg/g) [22], aloe vera leaf waste-based AC (29.11 mg/g) [23] and coconut shell-based AC (22.43 mg/g) [24].

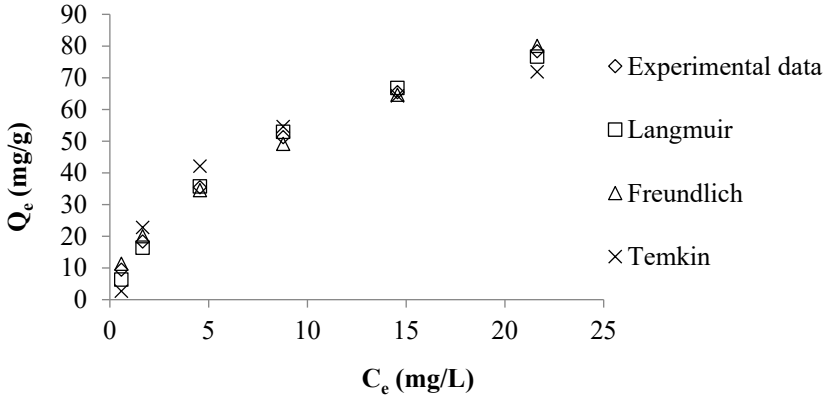

Figure 4: Isotherm plots for AMOX-SBAC adsorption system at 30°C

Table 4: Isotherm parameters for AMOX-SBAC adsorption system at 30°C

Langmuir	Values	Freundlich	Values	Temkin	Values
Q_m (mg/g)	110.52	n_F	1.85	A_T (L/mg)	1.99
K_L (L/mg)	0.11	K_F (mg/g)(L/mg)$^{1/n}$	15.21	B_T (L/mg)	19.10
RMSE	1.87	RMSE	1.58	RMSE	5.24
Error (%)	8.63	Error (%)	6.56	Error (%)	21.84

4. CONCLUSIONS

Sago bark-based activated carbon (SBAC) was successfully synthesized under the optimal conditions determined by response surface methodology (RSM): a radiation power of 556.41 watts, an activation time of 6.06 minutes, and an IR of 1.76 g/g. Under these parameters, SBAC achieved an amoxicillin (AMOX) uptake of 75.65 mg/g and a yield of 31.54%. The experimental results closely matched the predicted values, showing low error rates of 2.50% for AMOX uptake and 3.13% for yield, confirming the accuracy of the developed models. Regression analysis demonstrated strong model performance, with high R^2 values of 0.9675 for AMOX uptake and 0.9781 for SBAC yield, low standard deviations (SD) of 3.48 and 1.45, and high adequacy precision (AP) values of 21.21 and 26.65, respectively. Analysis of variance (ANOVA) results indicated that AMOX uptake was primarily influenced by radiation power and impregnation ratio (IR), while SBAC yield was extremely impacted by radiation power and radiation time. The optimized SBAC exhibited a Brunauer–Emmett–Teller (BET) surface area of 1011.93 m^2/g, a mesopore surface area of 738.65 m^2/g, a total pore volume of 0.3481 cm^3/g, and an average pore diameter of 2.79 nm, indicating mesoporous characteristics. Scanning electron microscopy (SEM) analysis confirmed a well-developed porous structure on the optimized SBAC surface, validating the effectiveness of the activation process. The adsorption of

AMOX onto the optimized SBAC followed the Freundlich isotherm model, suggesting multilayer adsorption with a maximum adsorption capacity (Q_m) of 110.52 mg/g. These findings highlight the strong potential of SBAC as an efficient and sustainable adsorbent for environmental remediation, particularly in the removal of pharmaceutical contaminants from wastewater, offering a promising pathway for cleaner water management using low-cost biomass resources. Future studies should explore the adsorption kinetics, thermodynamics, regeneration performance, and real wastewater applications of SBAC to further validate its potential for large-scale environmental remediation and sustainable water treatment systems.

Acknowledgements

This investigation is sponsored by Malaysian Ministry of Higher Education under the Fundamental Research Grant Scheme (project code: FRGS/1/2023/TK05/USM/02/8).

Author Contributions

All authors contributed toward data analysis, drafting and critically revising the paper and agree to be accountable for all aspects of the work.

Disclosure of Conflict of Interest

The authors have no disclosures to declare.

Compliance with Ethical Standards

The work adheres to the ethical standards, ensuring that all experimental procedures and methodologies were conducted with integrity and respect for ethical guidelines.

References

[1] Ighalo, J. O., Igwegbe, C. A., Aniagor, C. O. & Oba, S. N. (2021). A review of methods for the removal of penicillins from water. *Journal of Water Process Engineering,* 39, 101886.

[2] Lu, Z. Y., Ma, Y. L., Zhang, J. T., Fan, N. S., Huang, B. C. & Jin, R. C. (2020). A critical review of antibiotic removal strategies: Performance and mechanisms. *Journal of Water Process Engineering,* 38, 101681.

[3] Guerra, M. H., Alberola, I. O., Rodriguez, S. M., López, A. A., Merino, A. A. & Alonso, J. M. Q. (2019). Oxidation mechanisms of amoxicillin and paracetamol in the photo-Fenton solar process. *Water Research,* 156, 232-240.

[4] Mohamad, F. M. Y., Abdullah, A. Z. & Ahmad, M. A. (2024). Amoxicillin adsorption from aqueous solution by Cu(II) modified lemon peel based activated carbon: Mass transfer simulation, surface area prediction and F-test on isotherm and kinetic models. *Powder Technology,* 438, 119589.

[5] Ahammad, N. A., Yusop, M. F. M., Din, A. T. M. & Ahmad, M. A. (2021). Preparation of alpinia galanga stem based activated carbon via single-step microwave irradiation for cationic dye removal. *Sains Malaysiana,* 50(8), 2251-2269.

[6] Khan, M. N. N., Zainol, M. R. R. M. A., Yusop, M. F. M. & Ahmad, M. A. (2024). Turning waste into wonder: Arsenic removal using rice husk based activated carbon. *Journal of Engineering Research,* 13(3), 2503-2516.

[7] Yusop, M. F. M., Baharudin, M. H., Rashid, M. M., Alam, M. M. & Ahmad, M. A. (2025). Amoxicillin adsorption onto oil palm trunk-derived activated carbon: Synthesis optimization, modelling of mass transfer and ultrasonic regeneration. *Journal of Chemical Technology and Biotechnology,* 100(6), 1310-1327.

[8] Mohamad, F. M. Y., Abdullah, A. Z. & Ahmad, M. A. (2023). Adsorption of remazol brilliant blue R dye onto jackfruit peel based activated carbon: Optimization and simulation for mass transfer and surface area prediction. *Inorganic Chemistry Communications,* 158, 111721.

[9] Yusop, M. F. M., Jaya, E. M. J., Din, A. T. M., Bello, O. S. & Ahmad, M. A. (2022). Single-stage optimized microwave-induced activated carbon from coconut shell for cadmium adsorption. *Chemical Engineering and Technology,* 45(11), 1943-1951.

[10] Mohamad, F. M. Y., Rashid, M. M., Alam, M. M. & Ahmad, M. A. (2025). Copper metal-functionalized carbon from rattan waste via microwave pyrolysis for enhanced chloramphenicol removal: Optimization and F-test study. *Particuology,* 100, 196-213.

[11] Daouda, M. M. A., Akowanou, A. V. O., Mahunon, S. E. R., Adjinda, C. K., Aina, M. P. & Drogui, P. (2021). Optimal removal of diclofenac and amoxicillin by activated carbon prepared from coconut shell through response surface methodology. *South African Journal of Chemical Engineering,* 38, 78-89.

[12] Firdaus, M. Y. M., Rashid, M. M., Alam, M. M. & Ahmad, M. A. (2025). Enhanced Cd^{2+} removal via deprotonated-mango trunk functionalized carbon: Optimization and F-test for linear and non-linear isotherm and kinetic models. *Chemical Engineering Research and Design,* 220, 96-116.

[13] Qi, G., Pan, Z., Zhang, X., Chang, S., Wang, H., Wang, M., Xiang, W. & Gao, B. (2023). Microwave biochar produced with activated carbon catalyst: Characterization and adsorption of heavy metals. *Environmental Research,* 216, 114732.

[14] Siruru, H., Syafii, W., Wistara, N. & Pari, G. (2019). Characteristics of sago pith and sago bark waste from Seram Island, Maluku, Indonesia. *Biodiversitas Journal of Biological Diversity,* 20(12), 3517-3526.

[15] Amin, N. M., Sabli, N., Izhar, S. & Yoshida, H. (2019). A review: Sago wastes and its applications. *Pertanika Journal of Science and Technology,* 27(4), 1841-1862.

[16] Firdaus, M. Y. M., Rashid, M. M., Alam, M. M. & Ahmad, M. A. (2025). Copper-modified surface of orange peel-derived activated carbon for amoxicillin removal: Mass transfer simulation, attraction mechanism, and regeneration studies. *Arabian Journal for Science and Engineering.*

[17] Yusop, M. F. M., Ahmad, M. A., Rosli, N. A., Gonawan, F. N. & Abdullah, S. J. (2021). Scavenging malachite green dye from aqueous solution using durian peel based activated carbon. *Malaysian Journal of Fundamental and Applied Sciences,* 17(1), 95-103.

[18] Beyan, S. M., Prabhu, S. V., Sissay, T. T. & Getahun, A. A. (2021). Sugarcane bagasse based activated carbon preparation and its adsorption efficacy on removal of BOD and COD from textile effluents: RSM based modeling, optimization and kinetic aspects. *Bioresource Technology Reports,* 14, 100664.

[19] Mahari, W. A. W., Zainuddin, N. F., Nik, W. M. N. W., Chong, C. T. & Lam, S. S. (2016). Pyrolysis recovery of waste shipping oil using microwave heating. *Energies,* 9(10), 780.

[20] Jiménez, G. D., Rodriguez, J., Stevens, L., Kostas, E. T. & Dodds, C. (2024). Microwave pyrolysis of waste biomass and synthesis of micro-mesoporous activated carbons: The role of textural properties for CO_2 and textile dye adsorption. *Chemical Engineering Journal,* 488, 150926.

[21] Firdaus, M. Y. M., Rashid, M. M., Alam, M. M. & Ahmad, M. A. (2025). Synthesis of deprotonated grape stem functionalized carbon for boosted Cu^{2+} adsorption – Optimization, interaction mechanism, and F-test analysis. *Microchemical Journal*, 218, 115795.

[22] Sukor, N. F. & Jusoh, R. (2025). Hybrid activated carbon/ maltodextrin-functionalized fibrous silica for acetaminophen and amoxicillin adsorption: Advanced statistical physics modelling. *Environmental Research*, 278, 121691.

[23] Hashemzadeh, F., Ariannezhad, M. & Derakhshandeh, S. H. (2022). Evaluation of cephalexin and amoxicillin removal from aqueous media using activated carbon produced from Aloe vera leaf waste. *Chemical Physics Letters,* 800, 139656.

[24] Zhao, S., Wang, S., Dang, J., Wang, W., Wang, X., Wu, M. & Hu, J. (2024). Study on the adsorption performance of amoxicillin by hydrothermally modified coconut shell activated carbon. *Journal of Chemical Technology and Biotechnology,* 99(5), 1191-1200.